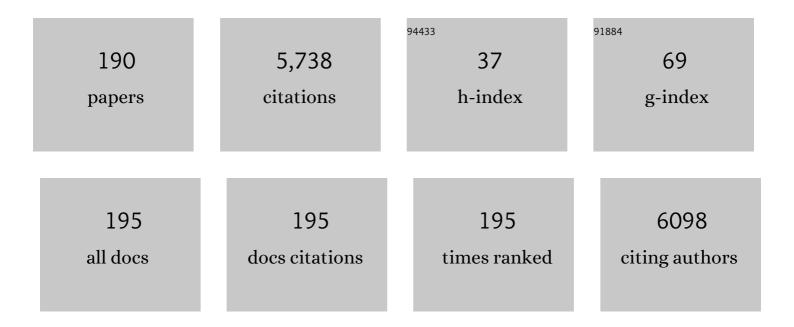
List of Publications by Year in descending order

Source: https://exaly.com/author-pdf/11481293/publications.pdf Version: 2024-02-01



<u> <u>Svo</u> Ματειιμισα</u>

#	Article	IF	CITATIONS
1	Tuning 2D magnetism in Fe3+XGeTe2 films by element doping. National Science Review, 2022, 9, .	9.5	7
2	Atomic insights into the ordered solid solutions of Ni and Au in ÎCu6Sn5. Acta Materialia, 2022, 224, 117513.	7.9	3
3	Phase Control of Solid-Solution Nanoparticles beyond the Phase Diagram for Enhanced Catalytic Properties. ACS Materials Au, 2022, 2, 110-116.	6.0	4
4	In Situ Observation of Liquid Solder Alloys and Solid Substrate Reactions Using High-Voltage Transmission Electron Microscopy. Materials, 2022, 15, 510.	2.9	3
5	Nitrile hydrogenation to secondary amines under ambient conditions over palladium–platinum random alloy nanoparticles. Catalysis Science and Technology, 2022, 12, 4128-4137.	4.1	7
6	Noble-Metal High-Entropy-Alloy Nanoparticles: Atomic-Level Insight into the Electronic Structure. Journal of the American Chemical Society, 2022, 144, 3365-3369.	13.7	94
7	Charge partitioning by intertwined metal-oxide nano-architectural networks for the photocatalytic dry reforming of methane. Chem Catalysis, 2022, 2, 321-329.	6.1	9
8	Crystal Structure Control of Binary and Ternary Solid-Solution Alloy Nanoparticles with a Face-Centered Cubic or Hexagonal Close-Packed Phase. Journal of the American Chemical Society, 2022, 144, 4224-4232.	13.7	40
9	Hydrogen sorption behaviour of Mg-5wt.%La alloys after the initial hydrogen absorption process. International Journal of Hydrogen Energy, 2022, 47, 16132-16143.	7.1	7
10	Quantitative Characterization of the Thermally Driven Alloying State in Ternary Ir–Pd–Ru Nanoparticles. ACS Nano, 2022, 16, 1612-1624.	14.6	5
11	Compositional dependence of structures and hydrogen evolution reaction activity of platinum-group-metal quinary RuRhPdIrPt alloy nanoparticles. Chemical Communications, 2022, 58, 6421-6424.	4.1	5
12	The Effect of Ru Precursor and Support on the Hydrogenation of Aromatic Aldehydes/Ketones to Alcohols. ChemCatChem, 2022, 14, .	3.7	1
13	Continuous-Flow Reactor Synthesis for Homogeneous 1 nm-Sized Extremely Small High-Entropy Alloy Nanoparticles. Journal of the American Chemical Society, 2022, 144, 11525-11529.	13.7	60
14	Co Nanoparticle Catalysts Encapsulated by BaO–La <sub>2</sub> O <sub>3</sub> Nanofractions for Efficient Ammonia Synthesis Under Mild Reaction Conditions. ACS Omega, 2022, 7, 24452-24460.	3.5	3
15	Boosting reverse water-gas shift reaction activity of Pt nanoparticles through light doping of W. Journal of Materials Chemistry A, 2021, 9, 15613-15617.	10.3	17
16	<i>In Situ</i> TEM Investigation of Structural Changes in Ni Nanoparticle Catalysts under Gas Atmospheres: Implications for Catalyst Degradation. ACS Applied Nano Materials, 2021, 4, 2175-2182.	5.0	6
17	Efficient overall water splitting in acid with anisotropic metal nanosheets. Nature Communications, 2021, 12, 1145.	12.8	124
18	Transition of Cationic Local Structures in Mg1-xNixAl2O4. Journal of Physical Chemistry C, 2021, 125, 5269-5277.	3.1	3

SYO MATSUMURA

#	Article	IF	CITATIONS
19	Atomic resolution imaging of cation ordering in niobium–tungsten complex oxides. Communications Materials, 2021, 2, .	6.9	11
20	Enhanced Hydrogenation Catalytic Activity of Ruthenium Nanoparticles by Solidâ€Solution Alloying with Molybdenum. European Journal of Inorganic Chemistry, 2021, 2021, 1186-1189.	2.0	3
21	Highly Stable and Active Solidâ€Solutionâ€Alloy Threeâ€Way Catalyst by Utilizing Configurationalâ€Entropy Effect. Advanced Materials, 2021, 33, e2005206.	21.0	22
22	Cu–Pd–B Alloy Nanoparticles Synthesized by External Boron Doping Method. Chemistry Letters, 2021, 50, 611-614.	1.3	1
23	First Observation of Superconductivity in Molybdenum–Ruthenium–Carbon Alloy Nanoparticles. Chemistry Letters, 2021, 50, 596-598.	1.3	1
24	Catalytic Roles and Synergetic Effects of Iron-Group Elements on Monometals and Alloys for Electrochemical Oxidation of Ammonia. Bulletin of the Chemical Society of Japan, 2021, 94, 1292-1299.	3.2	7
25	Mechanism of Hydrogen Storage and Structural Transformation in Bimetallic Pd–Pt Nanoparticles. ACS Applied Materials & Interfaces, 2021, 13, 23502-23512.	8.0	9
26	Interfacial reactions between Ga and Cu-xNi (x=0, 2, 6, 10, 14) substrates and the strength of Cu-xNi/Ga/Cu-xNi joints. Intermetallics, 2021, 133, 107168.	3.9	6
27	Rapid fabrication of tin-copper anodes for lithium-ion battery applications. Journal of Alloys and Compounds, 2021, 867, 159031.	5.5	9
28	Subpercent Local Strains Due to the Shapes of Gold Nanorods Revealed by Data-Driven Analysis. ACS Nano, 2021, 15, 12077-12085.	14.6	6
29	Fabrication of Integrated Copperâ€Based Nanoparticles/Amorphous Metal–Organic Framework by a Facile Sprayâ€Drying Method: Highly Enhanced CO 2 Hydrogenation Activity for Methanol Synthesis. Angewandte Chemie, 2021, 133, 22457-22462.	2.0	4
30	Fabrication of Integrated Copperâ€Based Nanoparticles/Amorphous Metal–Organic Framework by a Facile Sprayâ€Drying Method: Highly Enhanced CO <sub>2</sub> Hydrogenation Activity for Methanol Synthesis. Angewandte Chemie - International Edition, 2021, 60, 22283-22288.	13.8	29
31	Ni@onion-like carbon and Co@amorphous carbon: control of carbon structures by metal ion species in MOFs. Chemical Communications, 2021, 57, 5897-5900.	4.1	4
32	Nonequilibrium Flow-Synthesis of Solid-Solution Alloy Nanoparticles: From Immiscible Binary to High-Entropy Alloys. Journal of Physical Chemistry C, 2021, 125, 458-463.	3.1	18
33	Barium Oxide Encapsulating Cobalt Nanoparticles Supported on Magnesium Oxide: Active Non-Noble Metal Catalysts for Ammonia Synthesis under Mild Reaction Conditions. ACS Catalysis, 2021, 11, 13050-13061.	11.2	28
34	Properties of CuGa2 Formed Between Liquid Ga and Cu Substrates at Room Temperature. Journal of Electronic Materials, 2020, 49, 128-139.	2.2	29
35	Discovery of face-centred cubic Os nanoparticles. Chemical Communications, 2020, 56, 372-374.	4.1	20
36	Evidence of Copper Separation in Lithiated Cu <sub>6</sub> Sn <sub>5</sub> Lithium-Ion Battery Anodes. ACS Applied Energy Materials, 2020, 3, 141-145.	5.1	14

#	Article	IF	CITATIONS
37	Direct observation of the Ni stabilising effect in interfacial (Cu,Ni)6Sn5 intermetallic compounds. Materialia, 2020, 9, 100530.	2.7	8
38	Rational Synthesis for a Noble Metal Carbide. Journal of the American Chemical Society, 2020, 142, 1247-1253.	13.7	15
39	Coreduction methodology for immiscible alloys of CuRu solid-solution nanoparticles with high thermal stability and versatile exhaust purification ability. Chemical Science, 2020, 11, 11413-11418.	7.4	13
40	Significant Enhancement of Hydrogen Evolution Reaction Activity by Negatively Charged Pt through Light Doping of W. Journal of the American Chemical Society, 2020, 142, 17250-17254.	13.7	103
41	Electrochemically enhanced Cu6Sn5 anodes with tailored crystal orientation and ordered atomic arrangements for lithium-ion battery applications. Acta Materialia, 2020, 201, 341-349.	7.9	5
42	On the electronic structure and hydrogen evolution reaction activity of platinum group metal-based high-entropy-alloy nanoparticles. Chemical Science, 2020, 11, 12731-12736.	7.4	142
43	Platinum-Group-Metal High-Entropy-Alloy Nanoparticles. Journal of the American Chemical Society, 2020, 142, 13833-13838.	13.7	223
44	Statistical Evaluation of the Solid-Solution State in Ternary Nanoalloys. Journal of Physical Chemistry C, 2020, 124, 21843-21852.	3.1	2
45	Synthesis of Mo and Ru solid-solution alloy NPs and their hydrogen evolution reaction activity. Chemical Communications, 2020, 56, 14475-14478.	4.1	23
46	Effect of Calcination and Reduction Temperatures on the Catalytic Activity of Ru/La <sub>0.5</sub> Ce <sub>0.5</sub> O <sub>1.75</sub> for Ammonia Synthesis under Mild Conditions. Energy Technology, 2020, 8, 2000264.	3.8	11
47	Highly Correlated Size and Composition of Pt/Au Alloy Nanoparticles via Magnetron Sputtering onto Liquid. Langmuir, 2020, 36, 3004-3015.	3.5	16
48	Significantly enhanced CO oxidation activity induced by a change in the CO adsorption site on Pd nanoparticles covered with metal–organic frameworks. Chemical Communications, 2020, 56, 3839-3842.	4.1	7
49	Local structure investigations of accumulated damage in irradiated MgAl <sub>2</sub> O <sub>4</sub> . Journal of the American Ceramic Society, 2020, 103, 4654-4663.	3.8	6
50	Electron tomography imaging methods with diffraction contrast for materials research. Microscopy (Oxford, England), 2020, 69, 141-155.	1.5	19
51	Surface Dynamics for Creating Highly Active Ru Sites for Ammonia Synthesis: Accumulation of a Low-Crystalline, Oxygen-Deficient Nanofraction. ACS Sustainable Chemistry and Engineering, 2020, 8, 2726-2734.	6.7	50
52	Photocatalytic uphill conversion of natural gas beyond the limitation of thermal reaction systems. Nature Catalysis, 2020, 3, 148-153.	34.4	194
53	Intermetallic formation mechanisms and properties in room-temperature Ga soldering. Journal of Alloys and Compounds, 2020, 826, 154221.	5.5	17
54	Interfacial Reactions between Ga and Cu-10Ni Substrate at Low Temperature. ACS Applied Materials & Interfaces, 2020, 12, 21045-21056.	8.0	19

#	Article	IF	CITATIONS
55	Chemoselective hydrogenation of heteroarenes and arenes by Pd–Ru–PVP under mild conditions. RSC Advances, 2020. 10, 44191-44195. Atomic locations of minor dopants and their roles in the stabilization of (mml:math	3.6	11
56	xmlns:mml="http://www.w3.org/1998/Math/MathML"> <mml:mrow><mml:mi>η</mml:mi><mml:mtext>â°'mathvariant="normal"&gt;C<mml:msub><mml:mi mathvariant="normal"&gt;u<mml:mn>6</mml:mn></mml:mi </mml:msub><mml:mi mathvariant="normal"&gt;S<mml:msub><mml:mi< td=""><td>nl:mtext&gt;&lt; 2.4</td><td>mmi:mi 7</td></mml:mi<></mml:msub></mml:mi </mml:mtext></mml:mrow>	nl:mtext>< 2.4	mmi:mi 7
5 <b>7</b>	mathvariant="normal">n <mml:mn>5</mml:mn> . Physi The Effects of Trace Sb and Zn Additions on Cu6Sn5 Lithium-Ion Battery Anodes. Journal of Nanoscience and Nanotechnology, 2020, 20, 5182-5191.	0.9	3
58	Atom locations in a Ni doped Î~(Cu,Ni)6Sn5 intermetallic compound. Scripta Materialia, 2019, 158, 1-5.	5.2	22
59	Effects of Ni and Cu Antisite Substitution on the Phase Stability of CuGa2 from Liquid Ga/Cu–Ni Interfacial Reaction. ACS Applied Materials & Interfaces, 2019, 11, 32523-32532.	8.0	10
60	The effects of Ni on inhibiting the separation of Cu during the lithiation of Cu6Sn5 lithium-ion battery anodes. Journal of Power Sources, 2019, 440, 227085.	7.8	12
61	Lattice Tetragonality and Local Strain Depending on Shape of Gold Nanoparticles. Microscopy and Microanalysis, 2019, 25, 2122-2123.	0.4	1
62	Emergence of high ORR activity through controlling local density-of-states by alloying immiscible Au and Ir. Chemical Science, 2019, 10, 652-656.	7.4	50
63	Characterisation of lithium-ion battery anodes fabricated via in-situ Cu6Sn5 growth on a copper current collector. Journal of Power Sources, 2019, 415, 50-61.	7.8	34
64	Preparation and Growth Mechanism of Pt/Cu Alloy Nanoparticles by Sputter Deposition onto a Liquid Polymer. Langmuir, 2019, 35, 8418-8427.	3.5	15
65	Atomic structure observations and reaction dynamics simulations on triple phase boundaries in solid-oxide fuel cells. Communications Chemistry, 2019, 2, .	4.5	16
66	Solid-solution alloy nanoparticles of a combination of immiscible Au and Ru with a large gap of reduction potential and their enhanced oxygen evolution reaction performance. Chemical Science, 2019, 10, 5133-5137.	7.4	48
67	Structural and Thermodynamic Studies of Hydrogen Absorption/Desorption Processes on PdPt Nanoparticles. Journal of Physical Chemistry C, 2019, 123, 9471-9478.	3.1	3
68	A comparative characterization of defect structure in NiCo and NiFe equimolar solid solution alloys under in situ electron irradiation. Scripta Materialia, 2019, 166, 96-101.	5.2	5
69	Epitaxial GaAs/AlGaAs core–multishell nanowires with enhanced photoluminescence lifetime. Nanoscale, 2019, 11, 6859-6865.	5.6	10
70	Frontispiz: A CO Adsorption Site Change Induced by Copper Substitution in a Ruthenium Catalyst for Enhanced CO Oxidation Activity. Angewandte Chemie, 2019, 131, .	2.0	0
71	Charge transfer dependence on CO <sub>2</sub> hydrogenation activity to methanol in Cu nanoparticles covered with metal–organic framework systems. Chemical Science, 2019, 10, 3289-3294.	7.4	77
72	Frontispiece: A CO Adsorption Site Change Induced by Copper Substitution in a Ruthenium Catalyst for Enhanced CO Oxidation Activity. Angewandte Chemie - International Edition, 2019, 58, .	13.8	1

SYO MATSUMURA

#	Article	IF	CITATIONS
73	Sequential transmission electron microscopy observation of the shape change of gold nanorods under pulsed laser light irradiation. Microscopy (Oxford, England), 2019, 68, 174-180.	1.5	7
74	Strong Phonon–Phonon Interactions Securing Extraordinary Thermoelectric Ge <sub>1–<i>x</i></sub> Sb <sub><i>x</i></sub> Te with Zn-Alloying-Induced Band Alignment. Journal of the American Chemical Society, 2019, 141, 1742-1748.	13.7	199
75	Coating of 2D Flexible Metal–Organic Frameworks on Metal Nanocrystals. Chemistry Letters, 2019, 48, 173-176.	1.3	3
76	A CO Adsorption Site Change Induced by Copper Substitution in a Ruthenium Catalyst for Enhanced CO Oxidation Activity. Angewandte Chemie, 2019, 131, 2252-2257.	2.0	11
77	A CO Adsorption Site Change Induced by Copper Substitution in a Ruthenium Catalyst for Enhanced CO Oxidation Activity. Angewandte Chemie - International Edition, 2019, 58, 2230-2235.	13.8	48
78	Kyushu University Ultramicroscopy Platform for Nanomaterial Developing. Materia Japan, 2019, 58, 746-753.	0.1	0
79	Characterising the polymorphic phase transformation at a localised point on a Cu6Sn5 grain. Materials Characterization, 2018, 138, 113-119.	4.4	37
80	Solidâ€5olution Alloy Nanoparticles of the Immiscible Iridium–Copper System with a Wide Composition Range for Enhanced Electrocatalytic Applications. Angewandte Chemie, 2018, 130, 4595-4599.	2.0	13
81	Selective control of fcc and hcp crystal structures in Au–Ru solid-solution alloy nanoparticles. Nature Communications, 2018, 9, 510.	12.8	90
82	Solidâ€5olution Alloy Nanoparticles of the Immiscible Iridium–Copper System with a Wide Composition Range for Enhanced Electrocatalytic Applications. Angewandte Chemie - International Edition, 2018, 57, 4505-4509.	13.8	86
83	Achieving <i>zT</i> > 2 in pâ€Type AgSbTe <sub>2â^'</sub> <i><sub>x</sub></i> Se <i><sub>x</sub></i> Alloys via Exploring the Extra Light Valence Band and Introducing Dense Stacking Faults. Advanced Energy Materials, 2018, 8, 1702333.	19.5	143
84	Efficient ammonia synthesis over a Ru/La <sub>0.5</sub> Ce <sub>0.5</sub> O <sub>1.75</sub> catalyst pre-reduced at high temperature. Chemical Science, 2018, 9, 2230-2237.	7.4	142
85	Atomic Insights into Phase Evolution in Ternary Transitionâ€Metal Dichalcogenides Nanostructures. Small, 2018, 14, e1800780.	10.0	13
86	Influence of the Crystal Structure of Titanium Oxide on the Catalytic Activity of Rh/TiO <sub>2</sub> in Steam Reforming of Propane at Low Temperature. Chemistry - A European Journal, 2018, 24, 8742-8746.	3.3	28
87	PM-26Atomic insights into the Ni-stabilized hexagonal Î(Cu,Ni)6Sn5 intermetallic compound. Microscopy (Oxford, England), 2018, 67, i48-i48.	1.5	0
88	Imaging the Polymorphic Transformation in a Single Cu6Sn5 Grain in a Solder Joint. Materials, 2018, 11, 2229.	2.9	15
89	Ru/La <sub>0.5</sub> Pr <sub>0.5</sub> O <sub>1.75</sub> Catalyst for Low-Temperature Ammonia Synthesis. ACS Sustainable Chemistry and Engineering, 2018, 6, 17258-17266.	6.7	57
	Arrays of Planar Vacancies in Superior Thermoelectric		_

Arrays of Planar Vacancies in Superior Thermoelectric 90 Ge<sub>1â^</sub><i><sub>x</sub></i><sub>a^<</sub></i><sub>y</sub></i><sub>x</sub></i>Materials, 2018, 8, 1801837.

#	Article	IF	CITATIONS
91	Crystal-phase control of GaAs–GaAsSb core–shell/axial nanowire heterostructures by a two-step growth method. Journal of Materials Chemistry C, 2018, 6, 6726-6732.	5.5	20
92	Double enhancement of hydrogen storage capacity of Pd nanoparticles by 20 at% replacement with Ir; systematic control of hydrogen storage in Pd–M nanoparticles (M = Ir, Pt, Au). Chemical Science, 2018, 9, 5536-5540.	7.4	37
93	The local structure in heavily boron-doped diamond and the effect this has on its electrochemical properties. Carbon, 2018, 137, 333-342.	10.3	44
94	The Electronic State of Hydrogen in the αâ€Phase of the Hydrogenâ€Storage Material PdH(D) <sub><i>x</i></sub> : Does a Chemical Bond Between Palladium and Hydrogen Exist?. Angewandte Chemie, 2018, 130, 9971-9975.	2.0	6
95	The Electronic State of Hydrogen in the αâ€Phase of the Hydrogenâ€Storage Material PdH(D) <sub><i>x</i></sub> : Does a Chemical Bond Between Palladium and Hydrogen Exist?. Angewandte Chemie - International Edition, 2018, 57, 9823-9827.	13.8	25
96	Nano-scale dislocations induced by self-vacancy engineering yielding extraordinary n-type thermoelectric Pb0.96-yInySe. Nano Energy, 2018, 50, 785-793.	16.0	51
97	Discovery of Hexagonal Structured Pd–B Nanocrystals. Angewandte Chemie, 2017, 129, 6678-6682.	2.0	3
98	Discovery of Hexagonal Structured Pd–B Nanocrystals. Angewandte Chemie - International Edition, 2017, 56, 6578-6582.	13.8	34
99	Reply to â€~Comments on "Evidence of the hydrogen release mechanism in bulk MgH2â€â€™. Scientific Reports, 2017, 7, 43720.	3.3	0
100	Solid-Solution Alloying of Immiscible Ru and Cu with Enhanced CO Oxidation Activity. Journal of the American Chemical Society, 2017, 139, 4643-4646.	13.7	94
101	Encapsulation of Bimetallic Metal Nanoparticles into Robust Zirconium-Based Metal-Organic Frameworks: Evaluation of the Catalytic Potential for Size-Selective Hydrogenation. Chemistry - A European Journal, 2017, 23, 3583-3594.	3.3	31
102	Mechanisms of radiation-induced segregation in CrFeCoNi-based single-phase concentrated solid solution alloys. Acta Materialia, 2017, 126, 182-193.	7.9	133
103	In-situ investigation of the hydrogen release mechanism in bulk Mg2NiH4. Journal of Power Sources, 2017, 341, 130-138.	7.8	55
104	Hydrogen storage and stability properties of Pd–Pt solid-solution nanoparticles revealed via atomic and electronic structure. Scientific Reports, 2017, 7, 14606.	3.3	30
105	Firstâ€Principles Calculation, Synthesis, and Catalytic Properties of Rh u Alloy Nanoparticles. Chemistry - A European Journal, 2017, 23, 57-60.	3.3	26
106	A low-crystalline ruthenium nano-layer supported on praseodymium oxide as an active catalyst for ammonia synthesis. Chemical Science, 2017, 8, 674-679.	7.4	149
107	Recent Trend of Transmission Electron Microscopy and Application to Green Nano-technology. Journal of MMIJ, 2017, 133, 58-67.	0.3	0
108	PM-16Atomic-Resolution Tomography of Metal Alloy Nanoparticles: The Effects of Reconstruction Parameters. Microscopy (Oxford, England), 2017, 66, i25-i25.	1.5	10

#	Article	IF	CITATIONS
109	Facile Synthesis of Size-controlled Rh Nanoparticles via Microwave-assisted Alcohol Reduction and Their Catalysis of CO Oxidation. Chemistry Letters, 2017, 46, 1254-1257.	1.3	16
110	PM-11Lattice Strain Analysis in Gold Nanorods by Means of Atomic Resolution HAADF-STEM Experiments and Molecular Dynamics Simulations. Microscopy (Oxford, England), 2017, 66, i23-i23.	1.5	0
111	Image contrast enhancement of Ni/YSZ anode during the sliceâ€andâ€view process in FIBâ€SEM. Journal of Microscopy, 2016, 261, 326-332.	1.8	5
112	Three-Dimensional Imaging of a Long-Period Stacking Ordered Phase in Mg <sub>97</sub> Zn <sub>1</sub> Gd <sub>2</sub> Using High-Voltage Electron Microscopy. Materials Transactions, 2016, 57, 918-921.	1.2	3
113	Transmission electron microscopy of bulk specimens over 10 Âμm in thickness. Ultramicroscopy, 2016, 162, 10-16.	1.9	25
114	Effect of trace Na additions on the hydrogen absorption kinetics of Mg <sub>2</sub> Ni. Journal of Materials Research, 2016, 31, 1316-1327.	2.6	17
115	Enhanced damage resistance and novel defect structure of CrFeCoNi under in situ electron irradiation. Scripta Materialia, 2016, 125, 5-9.	5.2	62
116	A Synthetic Pseudo-Rh: NOx Reduction Activity and Electronic Structure of Pd–Ru Solid-solution Alloy Nanoparticles. Scientific Reports, 2016, 6, 28265.	3.3	44
117	Temperature dependent evolution of dislocation loops in YSZ under high energy electron irradiation. Transactions of the Materials Research Society of Japan, 2016, 41, 319-323.	0.2	4
118	Detection of picometer-order atomic displacements in drift-compensated HAADF-STEM images of gold nanorods. Microscopy (Oxford, England), 2016, 65, 391-399.	1.5	12
119	Observation of Dislocations in Thick Specimens Using by The High-Voltage Electron Microscopy with an Energy Filter. Materia Japan, 2016, 55, 597-597.	0.1	0
120	Atomic Displacements in Twinned Structures in a Gold Nanoparticle Irradiated with a Pulsed Laser Light. Materia Japan, 2016, 55, 583-583.	0.1	0
121	Kinetics of Ordered Domain Formation in Binary Alloys of D0 <sub>19</sub> Type Order. Transactions of the Materials Research Society of Japan, 2015, 40, 325-329.	0.2	2
122	Dual Lewis Acidic/Basic Pd <sub>0.5</sub> Ru <sub>0.5</sub> –Poly( <i>N</i> â€vinylâ€2â€pyrrolidone) Alloyed Nanoparticle: Outstanding Catalytic Activity and Selectivity in Suzuki–Miyaura Crossâ€Coupling Reaction. ChemCatChem, 2015, 7, 3887-3894.	3.7	25
123	Observation of the Ni/YSZ Interface in a Conventional SOFC. Journal of the Electrochemical Society, 2015, 162, F750-F754.	2.9	13
124	B22-P-06Ni/YSZ Interface in A Conventional Solid Oxide Fuel Cell. Microscopy (Oxford, England), 2015, 64, i105.2-i105.	1.5	0
125	B21-P-01STEM study of bimetallic Pd-Ru nanoparticles. Microscopy (Oxford, England), 2015, 64, i97.2-i97.	1.5	0
126	Preparation of solid–solution type Fe–Co nanoalloys by synchronous deposition of Fe and Co using dual arc plasma guns. Dalton Transactions, 2015, 44, 15764-15768.	3.3	16

SYO MATSUMURA

#	Article	IF	CITATIONS
127	Evidence of the hydrogen release mechanism in bulk MgH2. Scientific Reports, 2015, 5, 8450.	3.3	66
128	Atomically mixed Fe-group nanoalloys: catalyst design for the selective electrooxidation of ethylene glycol to oxalic acid. Physical Chemistry Chemical Physics, 2015, 17, 11359-11366.	2.8	23
129	Kinetics of the β → α Transformation of Tin: Role of α-Tin Nucleation. Crystal Growth and Design, 2015, 15, 5767-5773.	3.0	12
130	<i>In situ</i> observation of structural transformation of gold nanorods under pulsed laser irradiation in an HVEM. Microscopy (Oxford, England), 2014, 63, 261-268.	1.5	12
131	Multi-scale 3D characterization of long period stacking ordered structure in Mg-Zn-Gd cast alloys. Microscopy (Oxford, England), 2014, 63, i25.2-i26.	1.5	1
132	Encapsulation of Bimetallic Nanoparticles into a Metal–Organic Framework: Preparation and Microstructure Characterization of Pd/Au@ZIFâ€8. European Journal of Inorganic Chemistry, 2014, 2014, 5514-5521.	2.0	52
133	An ordered bcc CuPd nanoalloy synthesised via the thermal decomposition of Pd nanoparticles covered with a metal–organic framework under hydrogen gas. Chemical Communications, 2014, 50, 13750-13753.	4.1	28
134	Solid Solution Alloy Nanoparticles of Immiscible Pd and Ru Elements Neighboring on Rh: Changeover of the Thermodynamic Behavior for Hydrogen Storage and Enhanced CO-Oxidizing Ability. Journal of the American Chemical Society, 2014, 136, 1864-1871.	13.7	229
135	Shape-Dependent Hydrogen-Storage Properties in Pd Nanocrystals: Which Does Hydrogen Prefer, Octahedron (111) or Cube (100)?. Journal of the American Chemical Society, 2014, 136, 10222-10225.	13.7	104
136	Microstructure evolution of NiO–YSZ cermet during sintering. Solid State Ionics, 2014, 262, 460-464.	2.7	13
137	Hydrogen storage in Pd nanocrystals covered with a metal–organic framework. Nature Materials, 2014, 13, 802-806.	27.5	412
138	CO2-Free Power Generation on an Iron Group Nanoalloy Catalyst via Selective Oxidation of Ethylene Glycol to Oxalic Acid in Alkaline Media. Scientific Reports, 2014, 4, 5620.	3.3	36
139	Enhanced magnetization in highly crystalline and atomically mixed bcc Fe–Co nanoalloys prepared by hydrogen reduction of oxide composites. Nanoscale, 2013, 5, 1489.	5.6	27
140	Discovery of Face-Centered-Cubic Ruthenium Nanoparticles: Facile Size-Controlled Synthesis Using the Chemical Reduction Method. Journal of the American Chemical Society, 2013, 135, 5493-5496.	13.7	290
141	Application of TDGL Model to B2 Type Ordering with Two Step Phase Separation in Fe-Ni-Al Alloys. Materials Research Society Symposia Proceedings, 2013, 1535, 5601.	0.1	0
142	Atomistic observation of electron irradiation-induced defects in CeO <sub>2</sub> . Materials Research Society Symposia Proceedings, 2013, 1514, 93-98.	0.1	5
143	Atomic-Resolution X-ray Energy-Dispersive Spectroscopy Chemical Mapping of Substitutional Dy Atoms in a High-Coercivity Neodymium Magnet. Japanese Journal of Applied Physics, 2013, 52, 050201.	1.5	17
144	Simulations of structure formation in B2 type ordering with two step phase separation in Fe-Ni-Al alloys. , 2013, , .		0

#	Article	IF	CITATIONS
145	Development of Novel Optical Fiber System for Cathodoluminescence Detection in High Voltage Transmission Electron Microscope. Materials Transactions, 2013, 54, 854-856.	1.2	6
146	Detection of photons emitted from single erbium atoms in energy-dispersive X-ray spectroscopy. Nature Photonics, 2012, 6, 545-548.	31.4	57
147	Nanosize-Induced Drastic Drop in Equilibrium Hydrogen Pressure for Hydride Formation and Structural Stabilization in Pd–Rh Solid-Solution Alloys. Journal of the American Chemical Society, 2012, 134, 12390-12393.	13.7	59
148	Accumulation of radiation damage and disordering in MgAl <sub>2</sub> O <sub>4</sub> under swift heavy ion irradiation. International Journal of Materials Research, 2011, 102, 1082-1088.	0.3	20
149	Three-dimensional Visualization of Lattice Defects by Electron Tomography. Materia Japan, 2010, 49, 274-279.	0.1	4
150	Frenkel pair accumulation induced crystallization of amorphous MgAl2O4. Journal of Nuclear Materials, 2008, 378, 188-192.	2.7	17
151	Electron Tomography Imaging and Analysis of <i>γ</i> ′ and <i>γ</i> Domains in Niâ€based Superalloys. Advanced Materials, 2008, 20, 1905-1909.	21.0	31
152	High Resolution Observation of MgAl <sub>2</sub> O <sub>4</sub> Irradiated with 350 MeV Au ions. Materia Japan, 2008, 47, 614-614.	0.1	0
153	Three-Dimensional Observation of Superlattice Domains in Ordering Alloys by DFTEM Tomography. Nihon Kessho Gakkaishi, 2008, 50, 314-319.	0.0	1
154	Electron Enrgy-Dependent Type of Dislocation Loops in CeO <sub>2</sub> . Materia Japan, 2008, 47, 612-612.	0.1	0
155	Electron Tomography Observation of FePt Nanogranular Thin Films Irradiated with 210 MeV Xe Ions. Materia Japan, 2008, 47, 639-639.	0.1	0
156	In-situ Transmission Electron Microscopy Observation of Electron-beam-induced Defect-clusters in CaF <sub>2</sub> Crystal. Materia Japan, 2008, 47, 647-647.	0.1	0
157	The atomic structure of disordered ion tracks in magnesium aluminate spinel. Jom, 2007, 59, 27-30.	1.9	4
158	Tomographic Dark-Field TEM Observation of Ordered Ni;Mo Variants. Materia Japan, 2007, 46, 792-792.	0.1	1
159	Radiation Damage Effects in Insulators for Fusion Reactors: Microstructure Evolution in MgO-Al <sub>2</sub> O <sub>3</sub> System Oxide Crystals. Advances in Science and Technology, 2006, 45, 1961-1968.	0.2	0
160	Formation of Domain Structures in Ordering Processes of B2 and D03 Types. Materials Research Society Symposia Proceedings, 2006, 979, 1.	0.1	0
161	Dark-field transmission electron microscopy for a tilt series of ordering alloys: toward electron tomography. Microscopy (Oxford, England), 2005, 54, 373-377.	1.5	30
162	Effects of simultaneous displacive and ionizing radiations and of electric field on radiation damage in ionic crystals. Metallurgical and Materials Transactions A: Physical Metallurgy and Materials Science, 2004, 35, 2257-2266.	2.2	8

#	Article	IF	CITATIONS
163	TEM-Tomography Observation of Ion-Irradiated FePt Nano-Granular Films. Materia Japan, 2004, 43, 1003-1003.	0.1	0
164	Structural Disordering in Magnesium Aluminate Spinel Compounds under Ion-Beam Irradiation. Materials Research Society Symposia Proceedings, 2003, 792, 395.	0.1	0
165	Radiation-Induced Defects in α-Alumina Irradiated with Ions under an Applied Electric Field. Materia Japan, 2003, 42, 906-906.	0.1	Ο
166	Effects of Simultaneous Displacive and Ionizing Radiation in Ionic and Covalent Crystals. Defect and Diffusion Forum, 2002, 206-207, 53-74.	0.4	5
167	Atomistic Microstructures in Short-Range Ordered Alloys Nihon Kessho Gakkaishi, 2002, 44, 225-233.	0.0	1
168	Cation disordering in magnesium aluminate spinel crystals induced by electron or ion irradiation. Journal of Nuclear Materials, 2000, 283-287, 952-956.	2.7	48
169	Defect Clusters in Yttria-stabilized Cubic-zirconia Irradiated with Ions and/or Electrons. Materia Japan, 2000, 39, 993-993.	0.1	Ο
170	Short range order and its transformation to long range order in Ni4Mo. Acta Materialia, 1998, 46, 881-892.	7.9	48
171	Time-Evolution of Long Range Ordering in CuAuPd Ternary Alloys. Materials Transactions, JIM, 1998, 39, 159-168.	0.9	3
172	Recent Development in Quantitative Electron Diffraction for Crystallography of Materials. Materials Transactions, JIM, 1998, 39, 927-937.	0.9	3
173	Interpretation of High Resolution Transmission Electron Microscope Images of Short Range Ordered Ni <sub>4</sub> Mo. Materials Transactions, JIM, 1998, 39, 914-919.	0.9	4
174	Element Mapping Around Grain Boundaries in Ca-doped β-Si <sub>3</sub> N <sub>4</sub> by Electron Spectroscopic Imaging. Materia Japan, 1998, 37, 981-981.	0.1	0
175	Microstructure of CuAu-I-type ordered phase in III-V semiconductor alloys grown on a (001) substrate. Physical Review B, 1996, 54, 10814-10819.	3.2	6
176	Quantitative Analysis of Ordered Structure in Multinary Alloys by the IKL-ALCHEMI Method and Its Application to Ordering Kinetics. Journal of Electron Microscopy, 1996, 45, 93-98.	0.9	5
177	Kinetics of irradiation-induced phase transformations in tricritical systems. Physical Review B, 1996, 54, 6184-6193.	3.2	12
178	Monte Carlo simulation of CuPtâ€ŧype ordering in offâ€stoichiometric IIIâ€V semiconductor alloys. Journal of Applied Physics, 1995, 77, 2370-2374.	2.5	14
179	Diffuse scattering in partially ordered III-V semiconductor alloys. Physical Review B, 1995, 52, 5154-5159.	3.2	14
180	Kinetics of CuPt-type ordered phase formation in III-V semiconductor alloys during (001) epitaxial growth due to step flow. Physical Review B, 1995, 51, 9707-9714.	3.2	28

#	Article	IF	CITATIONS
181	An Analytical Electron Diffraction Technique for the Determination of Long-Range Order Parameters in Multi-Component Ordered Alloys. Materials Transactions, JIM, 1991, 32, 905-910.	0.9	12
182	Ordered Structures and Phase States in Epitaxial Layers of Ill–V Semiconductor Alloys. Japanese Journal of Applied Physics, 1990, 29, 688-695.	1.5	24
183	Dynamical Behavior of Ordering with Phase Separation in Off-Stoichiometric Fe <sub>3</sub> Si Alloys. Materials Transactions, JIM, 1989, 30, 695-706.	0.9	32
184	Study of temperature factors in cubic crystals by high-voltage electron diffraction. Journal of Electron Microscopy Technique, 1989, 12, 262-271.	1.1	10
185	Higher order Laue zone patterns in convergent beam electron diffraction and determinations of local lattice parameters in .ALPHA and .ALPHA.2-phases of a Cu-20at%Al alloy ISIJ International, 1989, 29, 191-197.	1.4	6
186	Effect of Spatial Correlation of Particles on Ostwald Ripening. , 1988, , 233-238.		1
187	Dynamics of Ordering with Phase Separation in Iron-Silicon Alloys. , 1988, , 315-320.		1
188	Electron microscopic observation and its interpretation of Ostwald ripening in precipitation dynamics in alloys. Phase Transitions, 1987, 8, 213-225.	1.3	14
189	Precipitation Behavior in a Cu-4.5 wt%Co Alloy. Japanese Journal of Applied Physics, 1981, 20, L605-L608.	1.5	12
190	In-Situ Observation of Liquid Solder Alloys and Solid Substrate Reactions Using High-Voltage Transmission Electron Microscopy. SSRN Electronic Journal, 0, , .	0.4	0